molecular pharmaceutics

Article

pubs.acs.org/molecularpharmaceutics

Nanodiamond–Mitoxantrone Complexes Enhance Drug Retention in Chemoresistant Breast Cancer Cells

Tan-Boon Toh,[†,∥] Dong-Keun Lee,[§,∥] Weixin Hou,[†] Lissa Nurrul Abdullah,[†] Jacqueline Nguyen,[§] Dean Ho,*[,§] and Edward Kai-Hua Chow*[,†,‡]

[†]Cancer Science Institute of Singapore, National University of Singapore, Singapore

[‡]Department of Pharmacology, Yong Loo Lin School of Medicine, National University of Singapore, Singapore

[§]Division of Oral Biology and Medicine, Division of Advanced Prosthodontics, The Jane and Jerry Weintraub Center for Reconstructive Biotechnology, UCLA School of Dentistry, California NanoSystems Institute, and Jonsson Comprehensive Cancer Center, University of California, Los Angeles, Los Angeles, California 90095, United States

ABSTRACT: Chemoresistance is a prevalent issue that accounts for the vast majority of treatment failure outcomes in metastatic cancer. Among the mechanisms of resistance that markedly decrease treatment efficacy, the efflux of drug compounds by ATP-binding cassette (ABC) transporter proteins can impair adequate drug retention by cancer cells required for therapeutic cytotoxic activity. Of note, ABC transporters are capable of effluxing several classes of drugs that are clinical standards, including the anthracyclines such as doxorubicin, as well as anthracenediones such as mitoxantrone. To address this challenge, a spectrum of nanomaterials has been evaluated for improved drug retention and enhanced efficacy. Nanodiamonds (NDs) are emerging as a promising nanomaterial platform because they integrate several important properties into a single agent. These include a uniquely faceted truncated octahedral architecture that enables potent drug binding and dispersibility in water, scalably processed ND particles with uniform diameters of approximately 5 nm, and a demonstrated ability to improve drug tolerance while delaying tumor growth in multiple preclinical models, among others. This work describes a ND–mitoxantrone complex that can be rapidly synthesized and mediates marked improvements in drug efficacy. Comprehensive complex characterization reveals a complex with favorable drug delivery properties that is capable of improving drug retention and efficacy in an MDA-MB-231-luc-D3H2LN (MDA-MB-231) triple negative breast cancer cell line that was lentivirally transduced for resistance against mitoxantrone. Findings from this study support the further evaluation of ND–MTX in preclinical dose escalation and safety studies toward potentially clinical validation.

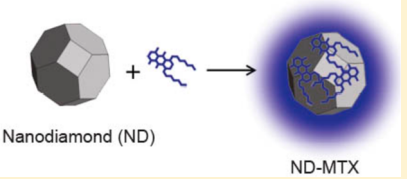

KEYWORDS: *nanodiamond, chemoresistance, mitoxantrone, ABCG2, breast cancer*

INTRODUCTION

Breast cancer is one of the leading causes of death in women worldwide, accounting for 14% of all cancer deaths in women.[1] Despite improved patient survival due to advances in targeted therapeutics, breast cancer patients often suffer relapse due to drug resistance mechanisms. One of the most frequently encountered drug resistant mechanisms involves the active efflux of drug from the cells, mediated primarily by transmembrane adenosine triphosphate (ATP)-dependent pumps called ATP-binding cassette (ABC) transporter proteins.[2] These drug transporters include the P-glycoprotein (ABCB1), the multidrug-resistance-associated protein (ABCC1), and the breast cancer related protein (BRCP) or ABCG2.[3,4] The *ABCG2* gene is an ABC half-transporter that is associated with resistance to mitoxantrone (MTX) and anthracyclines such as doxorubicin and its analogue, epirubicin.[5] It is well-established that many breast tumors that initially respond well to chemotherapy subsequently develop resistance to a broad range of drugs.[6] Currently, anthracycline-based chemotherapy, used in combination with 5-fluorouracil and cyclophosphamide is a standard treatment for metastatic breast cancer.[6]

Recently, nanomaterials have emerged as powerful tools for enhancing drug delivery and imaging.[7−12] Recent studies have demonstrated the use of nanoparticle-based drug carriers in combating chemoresistance in various cancer types.[13−20] To evaluate new therapeutic strategies in drug delivery, we examined the delivery of MTX adsorbed onto nanodiamonds (ND–MTX) in breast cancer cells. Nanodiamonds are chemically inert and scalably produced carbon particles with truncated octahedral architectures that are approximately 5 nm in diameter. NDs possess uniquely faceted surfaces that can release a broad spectrum of drugs in a sustained manner while improving therapeutic tolerance. More importantly, NDs possess excellent physical and chemical properties such as chemical stability in solution, good biocompatibility, and the ability to enhance therapeutic efficacy.[21−28] NDs have been shown to deliver anticancer chemotherapeutics, nucleic acids,

Special Issue: Drug Delivery and Reversal of MDR

Received: February 6, 2014
Revised: May 22, 2014
Accepted: May 27, 2014
Published: May 27, 2014

and insulin at an effective and sustained rate.[29−35] In particular, the use of ND−doxorubicin demonstrated the ability to overcome drug efflux and increase apoptosis in liver tumors *in vivo*.[30]

In this study, we explore the use of ND-mediated drug retention in drug-resistant breast cancer cells. NDs were engineered to reversibly bind and release the chemotherapeutic agent, MTX, via physical adsorption between the ND surface and MTX molecules. The resultant complex, ND−MTX was further characterized and compared with MTX drug alone. Importantly, we show that ND−MTX increased sensitivity of resistant breast cancer cells, possibly mediated via increased MTX retention in the cells. Additionally, we elucidated further the key mechanisms that influence ND drug release. This work suggests the use of NDs as a promising drug delivery platform for chemoresistant solid tumors.

EXPERIMENTAL SECTION

Cell Lines and Reagents. The MDA-MB-231-luc-D3H2LN (MDA-MB-231) breast cancer cell line was purchased from Caliper and maintained in Dulbecco's modified Eagle medium (DMEM) supplemented with 10% fetal bovine serum (FBS) with 1% sodium pyruvate and 1% nonessential amino acids in a humidified atmosphere at 37 °C with 5% CO_2. To generate MTX-resistant breast cancer cell line (MDA-MB-231-ABCG2), MDA-MB-231 cells were lentivirally transduced with pSIN4-EF2-ABCG2-IRES-Neo lentiviral vector (Addgene). Mitoxantrone (MTX) dihydrochloride and sodium hydroxide (NaOH) were purchased from Sigma-Aldrich (Milwaukee, USA). Nanodiamonds (ND) were obtained from the NanoCarbon Research Institute Ltd. (Nagano, Japan). DMEM and phosphate buffer saline (PBS) were obtained from Gibco, Life Technologies (NY, USA), and FBS was purchased from Gemini Bio Products (West Sacramento, USA). The NDs and all solutions were sterilized prior to use.

ND−MTX Loading and Optimization. Lyophilized MTX was dissolved in water at a stock concentration of 5 mg/mL and then subsequently diluted to a working stock of 1 mg/mL. NDs and MTX were mixed at a ratio of 5:1 (w/w) in the presence of NaOH (the final NaOH concentration in solution is 2.5 mM). The mixture was vortexed and incubated at room temperature. Subsequently, the mixture was centrifuged and washed with deionized water. The supernatant containing MTX was then removed. This supernatant was used to quantify the unbound MTX to calculate the loading efficiency of MTX bound to NDs. The pelleted ND−MTX was resuspended in deionized water by sonication. The loading of MTX on NDs was quantified by measuring the unbound MTX in the supernatant. The absorbance of MTX at 610 nm wavelength is linearly correlated with MTX concentration. A standard curve was established by serial dilution of MTX ranging from 0 to 200 μg/mL to attribute absorbance measurements due to MTX concentration.

MTX Release Profile from ND−MTX. MTX release from NDs was tested under different pH conditions by incubating ND−MTX (0.8 mg:0.16 mg/mL ND/MTX) in different pH solutions at a physiological condition of 37 °C. pH was adjusted using 1 M NaOH and 1 M HCl solutions. ND−MTX was resuspended in deionized water and different pH conditions (pH 2, 4, 7, 10, 12, and 7 with 50% FBS). ND−MTX was then centrifuged, and the resultant supernatant was used to quantify drug release at several time points (6, 12, 24, 48, and 72 h). In order to account for the stability of MTX at 37 °C, supernatant from each time point, as well as MTX standard curve samples, was stored at 37 °C, and MTX quantification was performed following collection of the final time point. The drug release assay was performed in triplicate. For the MTX release experiment carried out in DMEM with 50% FBS diluted 1:1 and 1:10 in PBS, solution containing 100 μg of MTX on NDs was initially removed by centrifugation for 20 min at 14 000 × *g* to obtain the ND−MTX pellet. This ND−MTX pellet was redispersed into 1 mL of 1:1 and 1:10 media by pipetting up and down gently, and then incubated at 37 °C. At each predetermined time period, ND−MTX was centrifuged for 20 min at 14 000 × *g*, and all supernatant was replaced with equal volume of fresh media. Each sample was also redispersed in media by pipetting up and down gently. To determine the amount of MTX released, UV absorption of MTX in the supernatant was measured at 610 nm, and calculated according to the MTX standard curve derived from the same release media. The drug release assay was performed in triplicate.

ND−MTX Chraacterization by FTIR, Dynamic Light Scattering (DLS), and ζ-Potential Measurement. Fourier transform infrared spectroscopy (FTIR) was performed using a PerkinElmer FTIR spectrum 2000 over a range of 400−4000 cm^{-1}. Samples were dried using a rotary evaporator. Two milligrams of sample was mixed with 0.1 g of potassium bromide (KBr) powder using mortar and pestle, after which the sample was pressed to a thin film before the spectra were taken. The analysis data were recorded on Jasco FT/IR-420 with the resolution of 1 cm^{-1} and 64 scan accumulations. The size and zeta (ζ) potential of ND and ND−MTX suspensions (0.2−0.3 mg/mL) were determined by using Zetasizer Nano ZS (Malvern Instrument, UK). Nanoparticle size measurements were performed at 25 °C and a 173° backscattering angle with at least 3 runs. The hydrodynamic diameter was determined by the average of *z*-average values with those standard deviations from 3 runs. Zeta potential was also measured at 25 °C in the aqueous medium by using DTS-1060C clear zeta cells in automatic mode.

Cell Viability and IC_{50} Calculations. Five × 10^4 cells were plated on a 96-well culture plate (NUNC) and cultured for 24 h at 37 °C. Equivalent MTX and ND−MTX drug concentrations were used so that informed comparisons could be made. MTX and ND−MTX (0.00001, 0.0001, 0.001, 0.005, 0.007, 0.01, 0.02, 0.04, 0.06, 0.08, 0.1, 0.2, 0.4, 0.6, 0.8, 1, 10, and 100 μM) were added per treatment condition (n = 3) for 4 h, after which cells were washed once with 1 × PBS. An additional wash was carried out after 24 h incubation, thereafter cells were further incubated with complete growth medium for 48 h before quantification of cell viability using 3-(4,5-dimethylthiazol-2-yl)-5-(3-carboxymethoxyphenyl)-2-(4-sulfophenyl)-2*H*-tetrazolium (MTS) colorimetric assay (Promega) at absorbance 490 nm according to manufacturer's instructions. Background absorbance (staining in the absence of the cells) was subtracted from each sample before calculating the absorbance ratio. Sigmoidal dose−response curves and IC_{50} values were generated by fitting calculated cell viability values at different log concentrations using Graphpad Prism 6 software (Graphpad, CA, USA) according to the four-parameter logistic sigmoidal dose−response curve: $Y = IC_{100} + (IC_0 - IC_{100})/(1 + 10^{(\log IC_{50} - X) \times \text{hill slope}})$ where X is the logarithm concentration and Y is the predicted response.

***In Vitro* MTX Retention Profile.** To visualize drug retention *in vitro*, 1 × 10^4 cells were plated on 8-well chamber slides (NUNC) and cultured for 24 h at 37 °C. The cells were

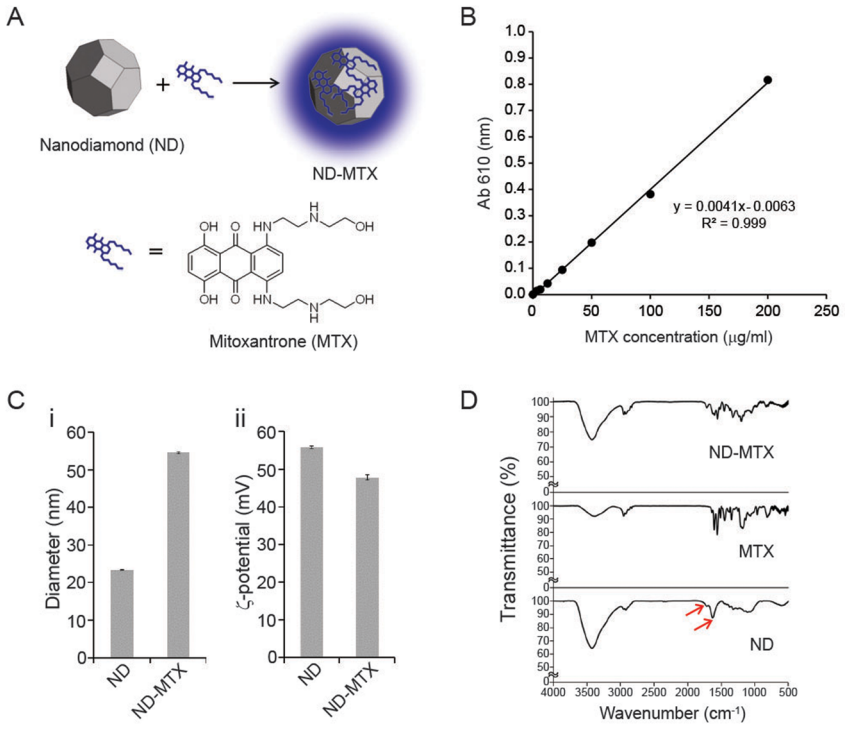

Figure 1. Physical characterization of ND−MTX. (A) Schematic diagram of MTX loading onto ND to form ND−MTX conjugate. (B) Standard curve of MTX loading efficiency on ND. (C) Particle size distribution (i) and zeta potential (ii) of ND and ND−MTX. (D) FITR spectra of ND, MTX, and ND−MTX. The FTIR spectra of ND−MTX showed distinctively C═C−H out of plane bending vibration at 820−840 cm^{-1}, C═C stretching vibration at 1560 and 1603 cm^{-1}, and C═O stretching vibration at 1628 cm^{-1} compared with that of ND. Those peaks are matched well with MTX.

synchronized for 2 h with serum-free medium prior treatment with IC_{50} of MTX or ND−MTX for 1 h. Thereafter, cells were washed once with 1 × PBS and incubated in complete growth media for 6 and 24 h. Cells were then washed with 1 × PBS and fixed with 4% paraformaldehyde (PFA) for 10 min at 37 °C. Subsequently, the fixed cells were stained with 4′,6-diamidino-2-phenylindole (DAPI) for 5 min and visualized using a Nikon confocal laser scanning microscope. Fixed cells were visualized with the DAPI channel at an excitation/emission wavelength of 345/455 nm, and intracellular MTX was visualized with the Cy5 channel at an excitation/emission wavelength of 610/685 nm.

Western Blot. Cells were pelleted and lysed in buffer containing 0.5% sodium deoxycholate, 1% NP-40 detergent, 0.1% SDS, 0.15 mol/L NaCl, and 10 mmol/L Tris-HCl (pH 7.4), with protease and phosphatase inhibitors cocktail tablets (Roche). Equal amounts of protein were separated by SDS-polyacrylamide gel electrophoresis, transferred to polyvinylidene difluoride membranes, and probed with primary antibodies. Membranes were processed according to standard procedures and proteins detected using the imaging system ImageQuant LAS 500 (GE healthcare Life Sciences). The following antibodies were used: anti-ABCG2 (1:1000, Cell Signaling) and anti-β-actin (1:5000, Cell Signaling).

Quantitative Real-Time PCR. Total RNA was extracted from cell pellet using TRI Reagent (Sigma-Aldrich) and reverse transcription was carried out in 20 μL reactions on 500 ng of total RNA from each sample using iScript Reverse Transcription Supermix (Bio-Rad Laboratories) according to manufacturers' instructions. For qPCR, triplicate aliquots of cDNA for each sample (2 μL) were then subjected to 40 amplification cycles of PCR (Applied Biosystems Prism 7500 sequence detection system) using iTaq Universal SYBR Green Supermix (Bio-Rad Laboratories). Primers used were as follow: *ABCG2* (forward primer, 5′-TGGCTTAGACTCAAGCACAGC-3′; reverse primer, 5′-TCGTCCCTGCTTAGACATCC-3′), *ABCB1* (forward primer, 5′- GCCTGGCAGCTGGAAGACAAATAC-3′; reverse primer, 5′- ATGGCCAAAATCACAAGGGTTAGC-3′), *ABCC1* (forward primer, 5′-GTACATTAACATGATCTGGTC-3′; reverse primer, 5′-CGTTCATCAGCTTGATCCGAT-3′), and *GAPDH* (forward primer, 5′-AGCCACATCGCTCAGACAC-3′; reverse primer, 5′-GCCCAATACGACCAAATCC-3′). The level of gene expression was determined using *GAPDH* as the normalizer gene and expressed as mean ± SD of the triplicate PCR reactions.

Statistical Analysis. Student *t* test or Mann−Whitney analysis were used for comparison of 2 independent groups. $P < 0.05$ was accepted as statistically significant. All experiments were at least performed in triplicate, the results averaged, and the standard deviation (SD) or standard error of the mean (SEM) calculated.

RESULTS

Physical Characterization of ND−MTX. ND−MTX was formed by mixing sterilized NDs and MTX at an optimal ratio of 5:1 (w/w) (Figure 1A). The loading efficiency of MTX on NDs was 87.2 ± 8.51 as measured by the absorbance of unbound MTX at 610 nm (Figure 1B).

After the initial optimization of MTX binding to NDs, ND−MTXs were characterized to verify successful loading. Physical characteristics such as particle size, surface-charge properties, and MTX release profiles were investigated. Dynamic light scattering (DLS) was used to determine the average hydro-

dx.doi.org/10.1021/mp5001108 | *Mol. Pharmaceutics* 2014, 11, 2683−2691

dynamic diameter of ND and ND−MTX agglomerates. As shown in Figure 1Ci, NDs suspended in water agglomerate into complexes with an average size of 23.3 ± 0.09 nm. After physical adsorption of MTX, the ND−MTX complexes equilibrated with an average diameter of 54.6 ± 0.29 nm, suggesting the additional layer of bound MTX on ND. In addition, NDs exhibited a surface charge of 55.8 ± 0.37 mV, whereas ND−MTX had a slight decrease in zeta-potential of 47.8 ± 0.66 mV (Figure 1 Cii). This suggests that the loading of MTX on ND will not have a significant effect on cellular permeability. Furthermore, the narrow size distribution and negligible change in zeta potentials between NDs and ND−MTXs indicate good homogeneity of the particles in solutions, which is a crucial physical property of translationally relevant drug delivery systems.

To further demonstrate the successful formation of ND−MTX, FITR spectra were evaluated to compare the peaks of ND, MTX, and ND−MTX (Figure 1D). Our FTIR spectra analysis on ND showed the broad stretching vibration band of C═O at 1700 to 1800 cm^{-1}, which is from various carbonyl groups formed on ND, such as ketone, ester, lactone, and carboxylic acid. The peak at 1632 cm^{-1} belongs to the bending vibration of O−H from adsorbed water on ND. Those peaks (indicated as red arrows) are consistent with previous findings. In addition, a majority of the peaks for ND−MTX coincided well with MTX, serving as evidence for the presence of MTX on ND. By comparing the spectra of ND and ND−MTX, the vibration bands at 820 to 840, 1560, 1603, and 1628 cm^{-1} at ND−MTX showed distinct signals, whereas ND did not show any vibration bands at these indicated regions. These distinct peaks are designated to C═C−H out of plane bending vibration, two peaks of C═C stretching vibrations, and C═O stretching vibration, respectively. Because of the conjugation with double bonds on benzene and other pi bonds, C═O stretching vibration was shown at a lower wavenumber than usual C═O stretching vibration. Collectively, our FITR spectra analysis confirms the loading of MTX onto ND platforms due to the strong presence of ND and MTX peaks in ND−MTX spectra.

***In Vitro* Release of MTX from ND−MTX Conjugate.** Another key feature of a successful drug delivery system is the ability to release the drugs in a controlled biological setting. The release profile of MTX from ND−MTX was evaluated under a variety of pH conditions (Figure 2A). At basic conditions of pH 10 and 12, MTX was minimally released at 7.3 ± 3.2% and 2.5 ± 2.4%, respectively, after 6 h. At neutral (pH 7) and acidic (pH 4) conditions, the MTX release efficiency increased to 19 ± 3.8% and 37.5 ± 4.1%, respectively. At extreme acidic conditions of pH 2, about 54.8 ± 4.3% of MTX is released after the first 6 h of incubation, characteristic of a burst release. In addition, the *in vitro* drug release profile of ND−MTX was carried out in water (pH 7) plus 50% FBS as well as two different FBS-containing media (1:1 and 1:10 of DMEM (with 50% FBS)/PBS) in order to mimic the influence of biological matter, such as soluble proteins, salts, and sugars, on drug release. The addition of FBS to water resulted in an enhanced release of MTX (27.9 ± 3.2%) after the first 6 h of incubation (Figure 2A). As shown in Figure 2B, the presence of salts and sugars in DMEM as well as biological matter, such as soluble proteins in FBS, influenced drug release as early as 24 h with 49.6 ± 0.22% and 40.2 ± 1.83% in 1:1 and 1:10 of DMEM (50% FBS)/PBS media, respectively. ND−MTX demonstrated cumulative release of MTX over 3 weeks at 80.3 ± 0.33% (80 μg of MTX) and 62.0 ± 1.30% (62 μg of MTX) in 1:1 and 1:10 of DMEM (50% FBS)/PBS media, respectively.

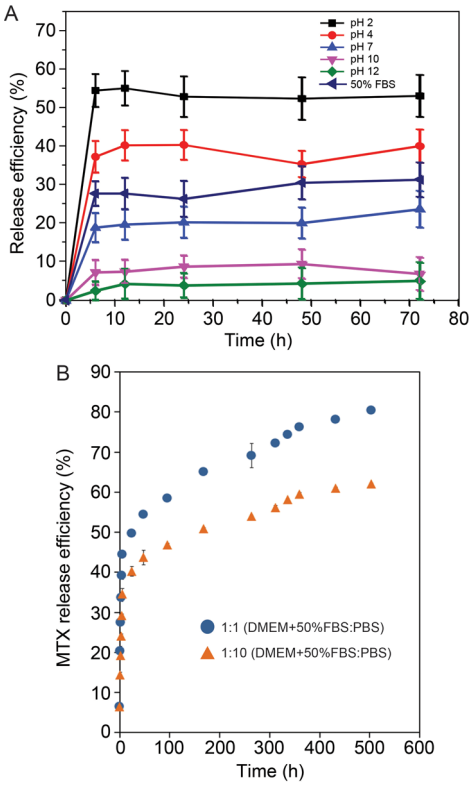

Figure 2. Release profile of MTX from ND−MTX conjugate. (A) *In vitro* release profile of MTX from ND−MTX complexes under various pH conditions. MTX elution was evaluated over a period of 72 h under pH 2, 4, 7, 10, 12, and pH 7 + 50% FBS conditions. MTX release behaviors displayed as percentage of total loaded MTX. (B) Release profile of MTX in 1:1 and 1:10 (DMEM (+50% FBS)/PBS). Higher FBS concentrations enhanced the release of MTX from ND−MTX. MTX release behaviors displayed as percentage of total loaded MTX.

Increased ABCG2 Expression in Drug-Resistant Breast Cancer Cells. A resistant breast cancer cell line was required to test the *in vitro* efficacy of the ND−MTX. To generate a drug-resistant breast cancer cell line variant, MDA-MB-231 cells were lentivirally transduced with a lentiviral vector over-expressing the drug transporter, ABCG2 (pSIN4-EF2-ABCG2-IRES-Neo).[36] We validated the mRNA overexpression of *ABCG2* by quantitative real time PCR. In addition, we also evaluated the mRNA expression levels of *ABCB1* and *ABCC1*, the two other most extensively studied ABC drug transporters. Our results showed that only *ABCG2* mRNA levels were significantly increased ($p < 0.01$) by 40-fold in MDA-MB-231-ABCG2 cells as compared to the MDA-MB-231 control cells (Figures 3A,B). Additionally, this increase in mRNA was confirmed by Western blot analysis to translate into an increase in ABCG2 protein expression (Figure 3A).

ND−MTX Efficacy Using IC_{50}. We next evaluated the half maximal inhibitory concentration or IC_{50} of MTX and ND−MTX to quantify the amount of therapeutics required to cause 50% cell death. Dose−response curves were generated over a wide range of therapeutic concentrations and fitted to a four-parameter logistic sigmoidal function. As illustrated in Figure 4A, MDA-MB-231-ABCG2 cells (MTX IC_{50}, 38 nM) were almost 2-fold more resistant to MTX compared to normal

dx.doi.org/10.1021/mp5001108 | *Mol. Pharmaceutics* 2014, 11, 2683−2691

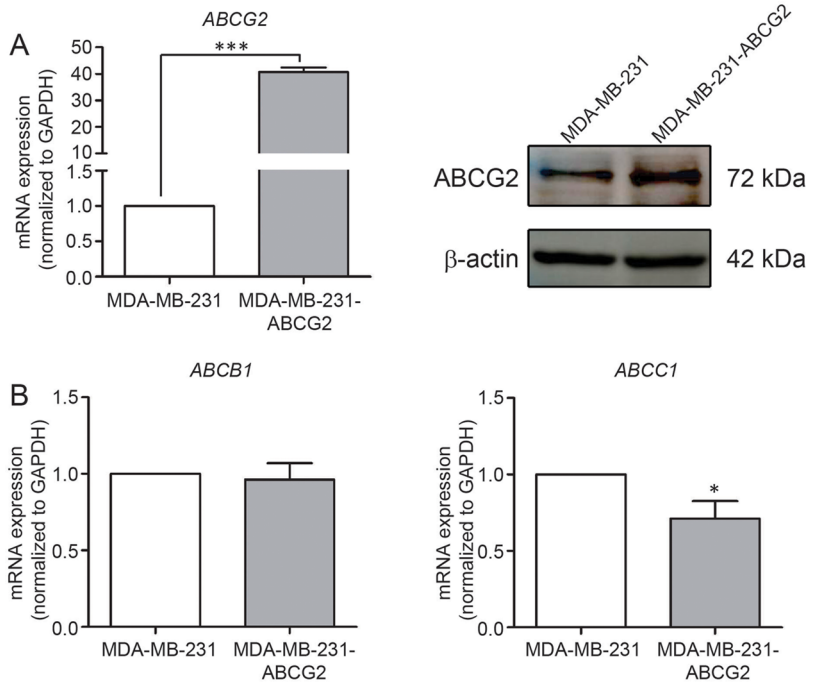

Figure 3. ABC transporter protein expression in breast cancer cells. (A) Gene expression analysis of *ABCG2* (left panel) and protein analysis of ABCG2 compared to control β-actin (right panel) in breast cancer cells (MDA-MB-231 and MDA-MB-231-ABCG2). (B) Gene expression analysis of two other major drug transporter proteins (*ABCB1* and *ABCC1*) of the ABC transporter family in breast cancer cells (MDA-MB-231 and MDA-MB-231-ABCG2).*, $p < 0.05$; ***, $p < 0.001$.

MDA-MB-231 cells (MTX IC_{50}, 20.1 nM), mainly attributed by the increased in *ABCG2* expression. Importantly, when similar comparison was made with ND−MTX, we observed a 6.4-fold decrease in IC_{50} in MDA-MB-231-ABCG2 cells when treated with ND−MTX compared to normal MDA-MB-231 cells, indicative of increased sensitivity of the drug-resistant cells to ND−MTX (Figure 4B). This increase in sensitivity of the therapeutics in drug-resistant MDA-MB-231-ABCG2 cells suggests the slow release of MTX from ND−MTX complexes can prolong MTX retention.

NDs Prolongs MTX Retention *in Vitro*. To confirm that ND delivery of MTX can improve MTX retention, we examined MTX retention at 6 and 24 h after 1 h of MTX treatment with MTX or ND−MTX. At 6 h, both MTX and ND−MTX showed visible retention in the cells, with ND−MTX exhibiting higher drug retention efficiency 35 ± 9.6% compared to MTX retention at 14 ± 4.8% (Figure 5Ai,Bi, $p = 0.0181$). At 24 h, cells treated with ND−MTX showed significantly higher retention than MTX. The retention efficiency for ND−MTX and MTX after 24 h was 39 ± 5.4% and 6 ± 1.9%, respectively (Figures 5Aii,Bii, $p = 0.004$). These significant differences demonstrated that NDs can enhance MTX retention *in vitro*, possibly accounting for the increased sensitivity of resistant breast cancer cells to MTX. Collectively, our *in vitro* drug retention study provides strong evidence for the use of ND−MTX as an effective drug delivery platform.

DISCUSSION

The focus of this study evaluates the efficiency of ND-based drug delivery agent (ND−MTX) in chemoresistant breast cancer cells. Active drug efflux across the cell membrane against the concentration gradient has been associated with the development of drug resistance and the subsequent reduction of intracellular drug concentrations cause insensitivity to chemotherapeutics and consequent treatment failure. One of the major drug transporters of MTX is the *ABCG2* gene product, which functions as an ATP-dependent membrane transporter. Overexpression of *ABCG2* has been shown to confer a drug resistant phenotype associated with an enhanced drug efflux capability.[37] Henceforth, developing strategies to overcome drug resistance becomes increasingly important to improve treatment efficacy.

To effectively deliver chemotherapeutics into cancer cells overexpressing drug transporters, we explored the use of an ND−drug complex platform. Nanoparticles possess the ability to shuttle their cargo in and out of the cells primarily through the process of endocytosis, thereby evading the drug transporter proteins, resulting in improved drug efficacy. Constant-pH dynamic simulations and experiments have previously demonstrated an important role for pH in the adsorption of cancer therapeutics onto NDs.[38] In our current study, we demonstrated that NDs effectively bind to MTX with high loading efficiency under high pH. Additionally, pH plays an important role in the removal of MTX from ND surface as the ND−MTX release profile showed greater release in acidic pH conditions. This will further ensure the proper release of MTX into the cells after endocytosis, where pH conditions of the endosomes and lysosomes are acidic. Furthermore, the ND−MTX complex showed a narrow size distribution, as indicated by the narrow width of the peak for ND−MTX. This is an important characteristic of consistent and scalable synthesis/processing procedures toward the development of novel clinical therapeutics. Additionally, the size of ND−MTX complexes fit within the optimal window for passive targeted nanoparticle cancer drug delivery, when relying on enhanced permeation and retention (EPR) effect.[13] As such, the physical characteristics of ND−MTX suggest suitability in the clinic.

dx.doi.org/10.1021/mp5001108 | *Mol. Pharmaceutics* 2014, 11, 2683−2691

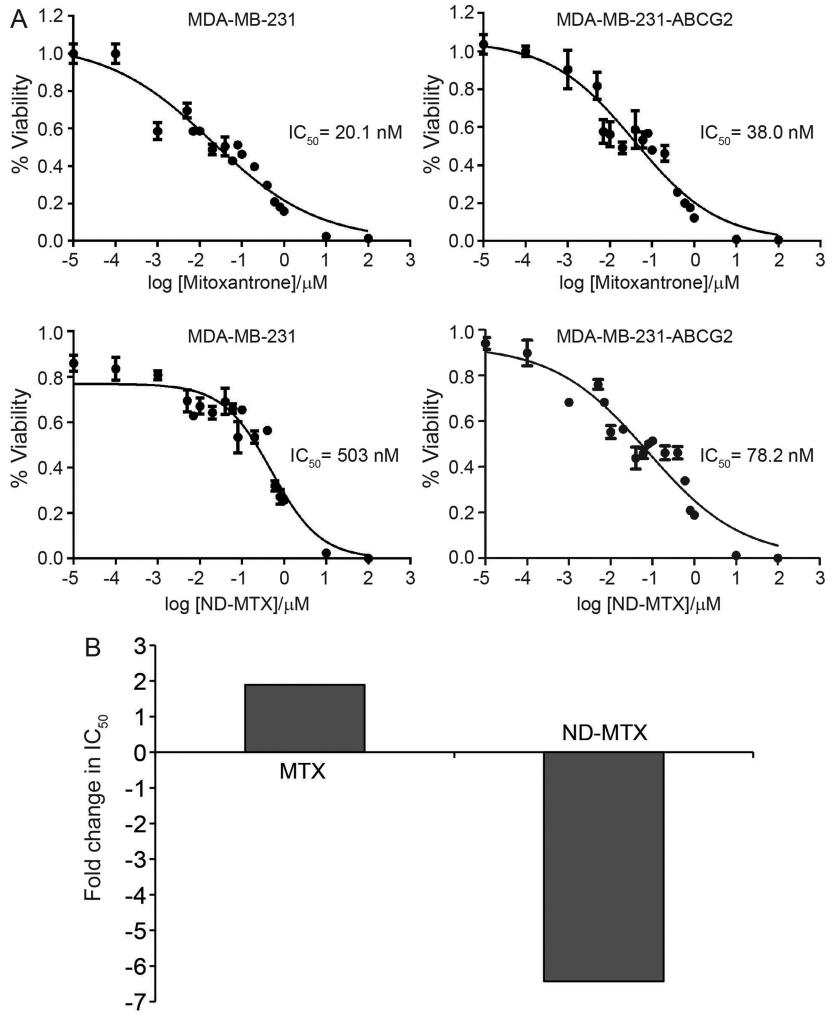

Figure 4. *In vitro* efficacy of MTX and ND−MTX in breast cancer cells. (A) Dose−response curves of MDA-MB-231 and MDA-MB-231-ABCG2 after exposure to a range of MTX or ND−MTX concentrations. (B) Fold change in IC_{50} values of MTX and ND−MTX for MDA-MB-231-ABCG2 cells relative to MDA-MB-231 control cells.

With regards to the drug release mechanism, prior studies have evaluated the interaction of water and proteins with the ND surface. Because the ND possesses a uniquely faceted truncated octahedral architecture, it has been previously shown that alternating electrostatics present between adjacent facets can mediate water molecule coordination around ND particles.[39] This mechanism may serve as the foundation for the markedly enhanced imaging properties observed with ND−gadolinium (Gd) magnetic resonance imaging agents that produced among the highest per-Gd relaxivity increases ever reported.[40] In addition to water coordination, protein interactions with ND surfaces have been previously studied.[41] In order to determine the effect of protein interaction on MTX release, ND−MTX were incubated with two different FBS containing media. In this work, we observed accelerated drug release in solutions with a higher FBS concentration, which may be attributed to the replacement of MTX by charged FBS proteins in the media. Similar to the mechanisms that enable potent water coordination on the ND surface, serum protein competition with the MTX compound may account for a more rapid replacement and subsequent elution of MTX. The modulation of release rate from the ND surface based on surrounding serum protein concentration warrants further investigation with regard to tuning the behavior of the ND platform.

Our *in vitro* dose−response study of MTX and ND−MTX on the drug resistant variant of MDA-MB-231 cells demonstrated the enhanced efficacy of ND−MTX in terms of improving sensitivity of the resistant cancer cells to the chemotherapeutic. This suggests that ND−MTX complexes were able to sustain and promote a steady release of MTX within the cells after bypassing the drug transporters, highlighting the advantage of using NDs as chemotherapeutic carriers. More importantly, when we evaluated the MTX retention profile *in vitro*, we were able to observe a marked improvement of MTX retention in the cells. This further confirms our earlier postulation that the increased drug sensitivity is attributed by enhanced MTX retention.

Multidrug resistance (MDR) is commonly associated with the overexpression of P-glycoprotein (MDR1 or ABCB1). One of the substrates for MDR1 includes MTX, a commonly used antineoplastic agent with some clinical activity in the treatment of leukemia, lymphoma, ovarian, and breast cancers.[42−44] The fact that chemotherapeutic agents such as MTX are substrates for multiple classes of drug transporters renders a bigger challenge for oncologists to use chemotherapy in the treatment and management of many cancers. Recently, the focus has been

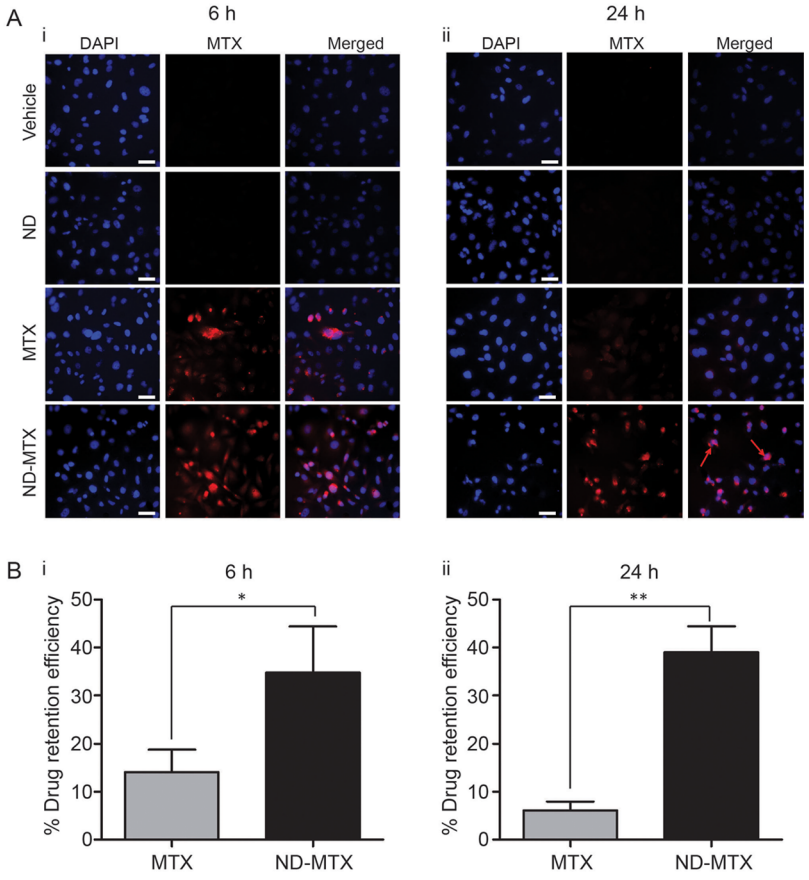

Figure 5. Conjugation of MTX to ND prolongs MTX retention in breast cancer cells. (A) Representative images of MTX retention at (i) 6 h and (ii) 24 h after 1 h of treatment with IC_{50} concentrations of MTX and ND−MTX. ND−MTX treatment at 24 h showed significant MTX retention (indicated by red arrows). (B) Quantitative scores of MTX retention efficiency at (i) 6 h and (ii) 24 h after 1 h of treatment with IC_{50} concentrations of MTX and ND−MTX.**, $p < 0.01$; *, $p < 0.05$. Scale bar represents 50 μm.

made on the reversal of MDR phenotype by inhibiting drug transporter proteins. However, most of the inhibitors have failed to produce clinically significant data due to issues with pharmacokinetic or pharmacodynamics interactions and toxicities.[45−47] Our work presented here is unique because drug delivery via the ND platform is independent of drug transporter proteins. Hence, the requirement to administer small molecule inhibitors of drug transporters in conjunction with chemotherapeutics is avoided, greatly reducing the potential side effects of poor pharmacokinetics and pharmacodynamics interactions.

These studies suggest that MTX delivery by NDs may have clinical benefits, particularly for patients with drug-resistant cancers or recurrence following chemotherapy treatment. Further preclinical dose escalation studies of ND−MTX and toxicity and excretion of studies of the ND platform, however, need to be further developed in relevant animal models before translation into clinical trials. In addition, further optimization of NDs for cell specific-targeted delivery of chemotherapeutic payloads can be developed to achieve specific targeting and further treatment efficacy.

■ CONCLUSIONS

This study realized an ND−MTX complex that mediated markedly enhanced MTX retention and improved therapeutic efficacy. In addition, the zeta potential of ND−MTX complexes and MTX did not vary significantly, hence minimizing the risk of repulsion near cellular membranes. The release of MTX from NDs was highly influenced by pH and soluble protein concentrations in the surrounding environment, suggesting a release mechanism amenable to biological delivery. More importantly, ND−MTX complexes showed enhanced sensitivity in the drug-resistant variant of breast cancer cells. Our *in vitro* study hence supports the continued evaluation of ND−MTX as an improved drug delivery platform for drug-resistant solid tumors.

■ AUTHOR INFORMATION

Corresponding Authors

*(D.H.) Tel: 1-310-825-7242. E-mail: dean.ho@ucla.edu.

*(E.K.-H.C.) Tel: +65 6516-8707. Fax: +65 6873 9664. E-mail: csikce@nus.edu.sg.

Author Contributions

‖T.-B.T. and D.-K.L. contributed equally to this work.

Notes

The authors declare no competing financial interest.

■ ACKNOWLEDGMENTS

E.K.-H.C. gratefully acknowledges support from the National Research Foundation Cancer Science Institute of Singapore RCE Main Grant, National Medical Research Council (NMRC CBRG-NIG BNIG12nov017), and Ministry of Education Academic Research Fund (MOE AcRF Tier 1 T1-2012 Oct-11). D.H. gratefully acknowledges support from the National Science Foundation CAREER Award (CMMI-0846323),

Center for Scalable and Integrated NanoManufacturing (DMI-0327077), CMMI-0856492, DMR-1105060, V Foundation for Cancer Research Scholars Award, Wallace H. Coulter Foundation Translational Research Award, Society for Laboratory Automation and Screening (SLAS) Endowed Fellowship, Beckman Coulter Life Sciences, and National Cancer Institute grant U54CA151880. The content is solely the responsibility of the authors and does not necessarily represent the official views of the National Cancer Institute or the National Institutes of Health.

■ ABBREVIATIONS USED

ND, nanodiamond; MTX, mitoxantrone; ABCG2, ATP-binding cassette subfamily G member 2; MDR, multidrug resistance; EPR, enhanced permeation and retention

■ REFERENCES

(1) Siegel, R.; Naishadham, D.; Jemal, A. Cancer Statistics, 2013. *CA Cancer J. Clin.* **2013**, *63*, 11−30.

(2) Allikmets, R.; Gerrard, B.; Hutchinson, A.; Dean, M. Characterization of the Human Abc Superfamily: Isolation and Mapping of 21 New Genes Using the Expressed Sequence Tags Database. *Hum. Mol. Genet.* **1996**, *5*, 1649−55.

(3) Gottesman, M. M.; Pastan, I. Biochemistry of Multidrug Resistance Mediated by the Multidrug Transporter. *Annu. Rev. Biochem.* **1993**, *62*, 385−427.

(4) Muller, M.; Meijer, C.; Zaman, G. J.; Borst, P.; Scheper, R. J.; Mulder, N. H.; de Vries, E. G.; Jansen, P. L. Overexpression of the Gene Encoding the Multidrug Resistance-Associated Protein Results in Increased Atp-Dependent Glutathione S-Conjugate Transport. *Proc. Natl. Acad. Sci. U.S.A.* **1994**, *91*, 13033−7.

(5) Ross, D. D.; Yang, W.; Abruzzo, L. V.; Dalton, W. S.; Schneider, E.; Lage, H.; Dietel, M.; Greenberger, L.; Cole, S. P.; Doyle, L. A. Atypical Multidrug Resistance: Breast Cancer Resistance Protein Messenger Rna Expression in Mitoxantrone-Selected Cell Lines. *J. Natl. Cancer Inst.* **1999**, *91*, 429−33.

(6) Wind, N. S.; Holen, I. Multidrug Resistance in Breast Cancer: From in Vitro Models to Clinical Studies. *Int. J. Breast Cancer* **2011**, *2011*, 967419.

(7) Eltoukhy, A. A.; Chen, D.; Alabi, C. A.; Langer, R.; Anderson, D. G. Degradable Terpolymers with Alkyl Side Chains Demonstrate Enhanced Gene Delivery Potency and Nanoparticle Stability. *Adv. Mater.* **2013**, *25*, 1487−93.

(8) Farokhzad, O. C.; Jon, S.; Khademhosseini, A.; Tran, T. N.; Lavan, D. A.; Langer, R. Nanoparticle-Aptamer Bioconjugates: A New Approach for Targeting Prostate Cancer Cells. *Cancer Res.* **2004**, *64*, 7668−72.

(9) Shin, S. R.; Bae, H.; Cha, J. M.; Mun, J. Y.; Chen, Y. C.; Tekin, H.; Shin, H.; Farshchi, S.; Dokmeci, M. R.; Tang, S.; Khademhosseini, A. Carbon Nanotube Reinforced Hybrid Microgels as Scaffold Materials for Cell Encapsulation. *ACS Nano* **2012**, *6*, 362−72.

(10) Perrault, S. D.; Chan, W. C. In Vivo Assembly of Nanoparticle Components to Improve Targeted Cancer Imaging. *Proc. Natl. Acad. Sci. U.S.A.* **2010**, *107*, 11194−9.

(11) Gil, P. R.; Parak, W. J. Composite Nanoparticles Take Aim at Cancer. *ACS Nano* **2008**, *2*, 2200−5.

(12) Zhang, X. Q.; Xu, X.; Lam, R.; Giljohann, D.; Ho, D.; Mirkin, C. A. Strategy for Increasing Drug Solubility and Efficacy through Covalent Attachment to Polyvalent DNA-Nanoparticle Conjugates. *ACS Nano* **2011**, *5*, 6962−70.

(13) Chow, E. K.; Ho, D. Cancer Nanomedicine: From Drug Delivery to Imaging. *Sci. Transl. Med.* **2013**, *5*, 216rv4.

(14) Davis, M. E.; Chen, Z. G.; Shin, D. M. Nanoparticle Therapeutics: An Emerging Treatment Modality for Cancer. *Nat. Rev. Drug Discovery* **2008**, *7*, 771−82.

(15) Vauthier, C.; Dubernet, C.; Chauvierre, C.; Brigger, I.; Couvreur, P. Drug Delivery to Resistant Tumors: The Potential of Poly(Alkyl Cyanoacrylate) Nanoparticles. *J. Controlled Release* **2003**, *93*, 151−60.

(16) Xu, X.; Xie, K.; Zhang, X. Q.; Pridgen, E. M.; Park, G. Y.; Cui, D. S.; Shi, J.; Wu, J.; Kantoff, P. W.; Lippard, S. J.; Langer, R.; Walker, G. C.; Farokhzad, O. C. Enhancing Tumor Cell Response to Chemotherapy through Nanoparticle-Mediated Codelivery of Sirna and Cisplatin Prodrug. *Proc. Natl. Acad. Sci. U.S.A.* **2013**, *110*, 18638−43.

(17) Meng, H.; Liong, M.; Xia, T.; Li, Z.; Ji, Z.; Zink, J. I.; Nel, A. E. Engineered Design of Mesoporous Silica Nanoparticles to Deliver Doxorubicin and P-Glycoprotein Sirna to Overcome Drug Resistance in a Cancer Cell Line. *ACS Nano* **2010**, *4*, 4539−50.

(18) Meng, H.; Mai, W. X.; Zhang, H.; Xue, M.; Xia, T.; Lin, S.; Wang, X.; Zhao, Y.; Ji, Z.; Zink, J. I.; Nel, A. E. Codelivery of an Optimal Drug/Sirna Combination Using Mesoporous Silica Nanoparticles to Overcome Drug Resistance in Breast Cancer in Vitro and in Vivo. *ACS Nano* **2013**, *7*, 994−1005.

(19) Jensen, S. A.; Day, E. S.; Ko, C. H.; Hurley, L. A.; Luciano, J. P.; Kouri, F. M.; Merkel, T. J.; Luthi, A. J.; Patel, P. C.; Cutler, J. I.; Daniel, W. L.; Scott, A. W.; Rotz, M. W.; Meade, T. J.; Giljohann, D. A.; Mirkin, C. A.; Stegh, A. H. Spherical Nucleic Acid Nanoparticle Conjugates as an Rnai-Based Therapy for Glioblastoma. *Sci. Transl. Med.* **2013**, *5*, 209ra152.

(20) Jin, X.; Mo, R.; Ding, Y.; Zheng, W.; Zhang, C. Paclitaxel-Loaded *N*-Octyl-*O*-Sulfate Chitosan Micelles for Superior Cancer Therapeutic Efficacy and Overcoming Drug Resistance. *Mol. Pharmaceutics* **2014**, *11*, 145−57.

(21) Lam, R.; Ho, D. Nanodiamonds as Vehicles for Systemic and Localized Drug Delivery. *Expert Opin. Drug Delivery* **2009**, *6*, 883−95.

(22) Kaur, R.; Badea, I. Nanodiamonds as Novel Nanomaterials for Biomedical Applications: Drug Delivery and Imaging Systems. *Int. J. Nanomed.* **2013**, *8*, 203−20.

(23) Zhu, Y.; Li, J.; Li, W.; Zhang, Y.; Yang, X.; Chen, N.; Sun, Y.; Zhao, Y.; Fan, C.; Huang, Q. The Biocompatibility of Nanodiamonds and Their Application in Drug Delivery Systems. *Theranostics* **2012**, *2*, 302−12.

(24) Ho, D. Beyond the Sparkle: The Impact of Nanodiamonds as Biolabeling and Therapeutic Agents. *ACS Nano* **2009**, *3*, 3825−9.

(25) Mochalin, V. N.; Shenderova, O.; Ho, D.; Gogotsi, Y. The Properties and Applications of Nanodiamonds. *Nat. Nanotechnol.* **2012**, *7*, 11−23.

(26) Lai, L.; Barnard, A. S. Modeling the Thermostability of Surface Functionalisation by Oxygen, Hydroxyl, and Water on Nanodiamonds. *Nanoscale* **2011**, *3*, 2566−75.

(27) Mochalin, V. N.; Pentecost, A.; Li, X. M.; Neitzel, I.; Nelson, M.; Wei, C.; He, T.; Guo, F.; Gogotsi, Y. Adsorption of Drugs on Nanodiamond: Toward Development of a Drug Delivery Platform. *Mol. Pharmaceutics* **2013**, *10*, 3728−35.

(28) Liang, Y.; Ozawa, M.; Krueger, A. A General Procedure to Functionalize Agglomerating Nanoparticles Demonstrated on Nanodiamond. *ACS Nano* **2009**, *3*, 2288−96.

(29) Moore, L.; Chow, E. K.; Osawa, E.; Bishop, J. M.; Ho, D. Diamond-Lipid Hybrids Enhance Chemotherapeutic Tolerance and Mediate Tumor Regression. *Adv. Mater.* **2013**, *25*, 3532−41.

(30) Chow, E. K.; Zhang, X. Q.; Chen, M.; Lam, R.; Robinson, E.; Huang, H.; Schaffer, D.; Osawa, E.; Goga, A.; Ho, D. Nanodiamond Therapeutic Delivery Agents Mediate Enhanced Chemoresistant Tumor Treatment. *Sci. Transl. Med.* **2011**, *3*, 73ra21.

(31) Alhaddad, A.; Adam, M. P.; Botsoa, J.; Dantelle, G.; Perruchas, S.; Gacoin, T.; Mansuy, C.; Lavielle, S.; Malvy, C.; Treussart, F.; Bertrand, J. R. Nanodiamond as a Vector for Sirna Delivery to Ewing Sarcoma Cells. *Small* **2011**, *7*, 3087−95.

(32) Shimkunas, R. A.; Robinson, E.; Lam, R.; Lu, S.; Xu, X.; Zhang, X. Q.; Huang, H.; Osawa, E.; Ho, D. Nanodiamond-Insulin Complexes as pH-Dependent Protein Delivery Vehicles. *Biomaterials* **2009**, *30*, 5720−8.

(33) Zhang, X. Q.; Chen, M.; Lam, R.; Xu, X.; Osawa, E.; Ho, D. Polymer-Functionalized Nanodiamond Platforms as Vehicles for Gene Delivery. *ACS Nano* **2009**, *3*, 2609−16.

(34) Huang, H.; Pierstorff, E.; Osawa, E.; Ho, D. Active Nanodiamond Hydrogels for Chemotherapeutic Delivery. *Nano Lett.* **2007**, *7*, 3305−14.
(35) Chen, M.; Pierstorff, E. D.; Lam, R.; Li, S. Y.; Huang, H.; Osawa, E.; Ho, D. Nanodiamond-Mediated Delivery of Water-Insoluble Therapeutics. *ACS Nano* **2009**, *3*, 2016−22.
(36) Zeng, H.; Park, J. W.; Guo, M.; Lin, G.; Crandall, L.; Compton, T.; Wang, X.; Li, X. J.; Chen, F. P.; Xu, R. H. Lack of Abcg2 Expression and Side Population Properties in Human Pluripotent Stem Cells. *Stem Cells* **2009**, *27*, 2435−45.
(37) Lee, J. S.; Scala, S.; Matsumoto, Y.; Dickstein, B.; Robey, R.; Zhan, Z.; Altenberg, G.; Bates, S. E. Reduced Drug Accumulation and Multidrug Resistance in Human Breast Cancer Cells without Associated P-Glycoprotein or Mrp Overexpression. *J. Cell Biochem.* **1997**, *65*, 513−26.
(38) Adnan, A.; Lam, R.; Chen, H.; Lee, J.; Schaffer, D. J.; Barnard, A. S.; Schatz, G. C.; Ho, D.; Liu, W. K. Atomistic Simulation and Measurement of pH Dependent Cancer Therapeutic Interactions with Nanodiamond Carrier. *Mol. Pharmaceutics* **2011**, *8*, 368−74.
(39) Osawa, E.; Ho, D.; Huang, H.; Korobov, M. V.; Rozhkova, N. N. Consequences of Strong and Diverse Electrostatic Potential Fields on the Surface of Detonation Nanodiamond Particles. *Diamond Relat. Mater.* **2009**, *18*, 904−909.
(40) Manus, L. M.; Mastarone, D. J.; Waters, E. A.; Zhang, X. Q.; Schultz-Sikma, E. A.; Macrenaris, K. W.; Ho, D.; Meade, T. J. Gd(III)-Nanodiamond Conjugates for Mri Contrast Enhancement. *Nano Lett.* **2010**, *10*, 484−9.
(41) Wang, H. D.; Niu, C. H.; Yang, Q.; Badea, I. Study on Protein Conformation and Adsorption Behaviors in Nanodiamond Particle-Protein Complexes. *Nanotechnology* **2011**, *22*, 145703.
(42) Stuart-Harris, R. C.; Smith, I. E. Mitoxantrone: A Phase II Study in the Treatment of Patients with Advanced Breast Carcinoma and Other Solid Tumours. *Cancer Chemother. Pharmacol.* **1982**, *8*, 179−82.
(43) Estey, E. H.; Keating, M. J.; McCredie, K. B.; Bodey, G. P.; Freireich, E. J. Phase II Trial of Mitoxantrone in Refractory Acute Leukemia. *Cancer Treat. Rep.* **1983**, *67*, 389−90.
(44) Lawton, F.; Blackledge, G.; Mould, J.; Latief, T.; Watson, R.; Chetiyawardana, A. D. Phase II Study of Mitoxantrone in Epithelial Ovarian Cancer. *Cancer Treat. Rep.* **1987**, *71*, 627−9.
(45) van der Holt, B.; Lowenberg, B.; Burnett, A. K.; Knauf, W. U.; Shepherd, J.; Piccaluga, P. P.; Ossenkoppele, G. J.; Verhoef, G. E.; Ferrant, A.; Crump, M.; Selleslag, D.; Theobald, M.; Fey, M. F.; Vellenga, E.; Dugan, M.; Sonneveld, P. The Value of the Mdr1 Reversal Agent Psc-833 in Addition to Daunorubicin and Cytarabine in the Treatment of Elderly Patients with Previously Untreated Acute Myeloid Leukemia (Aml), in Relation to Mdr1 Status at Diagnosis. *Blood* **2005**, *106*, 2646−54.
(46) Motzer, R. J.; Lyn, P.; Fischer, P.; Lianes, P.; Ngo, R. L.; Cordon-Cardo, C.; O'Brien, J. P. Phase I/II Trial of Dexverapamil Plus Vinblastine for Patients with Advanced Renal Cell Carcinoma. *J. Clin. Oncol.* **1995**, *13*, 1958−65.
(47) Nobili, S.; Landini, I.; Giglioni, B.; Mini, E. Pharmacological Strategies for Overcoming Multidrug Resistance. *Curr. Drug Targets* **2006**, *7*, 861−79.